HHS Public Access

Author manuscript

Carbon N Y. Author manuscript; available in PMC 2017 January 12.

Published in final edited form as:

Carbon N Y. 2016 January ; 96: 20–28. doi:10.1016/j.carbon.2015.09.040.

Thermochemistry and kinetics of graphite oxide exothermic decomposition for safety in large-scale storage and processing

Yang Qiu[a], **Felten Collin**[a], **Robert H. Hurt**[a,b], and **Indrek Külaots**[a,b,*]

[a]School of Engineering, Brown University, Providence, RI 02912, United States

[b]Institute for Molecular and Nanoscale Innovation, Brown University, Providence, RI 02912, United States

Abstract

The success of graphene technologies will require the development of safe and cost-effective nano-manufacturing methods. Special safety issues arise for manufacturing routes based on graphite oxide (GO) as an intermediate due to its energetic behavior. This article presents a detailed thermochemical and kinetic study of GO exothermic decomposition designed to identify the conditions and material compositions that avoid explosive events during storage and processing at large scale. It is shown that GO becomes more reactive for thermal decomposition when it is pretreated with OH^- in suspension and the effect is reversible by back-titration to low pH. This OH^- effect can lower the decomposition reaction exotherm onset temperature by up to 50 degrees of Celsius, causing overlap with common drying operations (100–120°C) and possible self-heating and thermal runaway during processing. Spectroscopic and modeling evidence suggest epoxide groups are primarily responsible for the energetic behavior, and epoxy ring opening/closing reactions are offered as an explanation for the reversible effects of pH on decomposition kinetics and enthalpies. A quantitative kinetic model is developed for GO thermal decomposition and used in a series of case studies to predict the storage conditions under which spontaneous self-heating, thermal runaway, and explosions can be avoided.

Graphical abstract

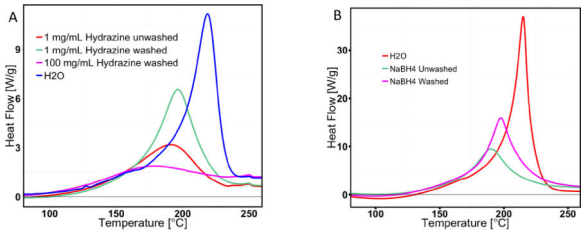

*Corresponding author. Tel: 401 863-2674, Indrek_Kulaots@brown.edu (Indrek Külaots).

Electronic supplementary information

Supplementary data associated with this article can be found in separate file titled ESI.

1. Introduction

Graphite oxide (GO) is the bulk raw product of graphite oxidation with strong oxidants that intercalate the graphite crystal lattice and introduce oxygen functional groups to the basal plane. GO has long been recognized as a thermally unstable, energetic material [1–13]. For example, Boehm et al. in 1962 reported “when heated quickly to about 180°C it deflagrates with production of a very voluminous fluffy carbon”, which “consists of very thin carbon sheets” [13].

Isolation of the graphene monolayer in 2004 [14–16] has greatly increased interest in this old material, GO, first for its role as an intermediate in the chemical route to graphene, and more recently as a precursor for solution exfoliation into graphene oxide as an end product. Graphene oxide is a hydrophilic water-processable two-dimensional monolayer material with its own applications (e.g. in membranes [17], emulsifiers [18], hydrogels [19], aerogels [20] and sorbents [21]), some of which are distinct from the applications of pristine graphene. GO is also of great interest as a bulk starting material for controlled thermal exfoliation into multilayer rGO flakes used as composite fillers [22–25]. High-aspect-ratio flakes achieve low percolation thresholds, and are thus especially attractive in conductive composites [22, 26, 27].

The current strong focus on graphene applications [28–32] together with the important role of GO as an intermediate in some processes, have now led to an intense interest in the large-scale manufacture and commercialization of bulk GO. With large-scale manufacturing also come scale-up issues, which include safety, and this motivates a much closer look at the behavior of GO as an energetic material under typical manufacturing and process conditions [5].

The thermal decomposition of GO yields large volumes of gaseous products, typically from 40 up to 60% per mass of the original sample mass depending on initial C:O ratio. The decomposition is highly exothermic and accompanied by self-heating, which for bulk samples above a critical size can lead to significant heat accumulation and thermal runaway reaction. If this occurs spontaneously in an unexpected or undesired processing or storage step, it can lead to gas release, vessel overpressure [5, 10], or ignition of the volatile gases with atmospheric oxygen and large-scale fire hazard [6].

This study addresses important unresolved issues that impact GO processing safety at large scale. First there is an unexplained large variation in GO decomposition exotherm onset temperatures. The onset temperature marks the practical start of the self-heating process and defines the maximum temperature for safe storage and processing. Many studies report onset temperatures in the range of 150–220°C [10, 11, 33, 34], but our preliminary data also identifies samples with onset temperatures near 100°C, which coincides with typical condition used in common drying operations [8, 35, 36]. What causes low GO decomposition onset temperature in some samples, and how can it be avoided? Secondly, there is a relatively large variation in the reported magnitudes of the exotherm ranging from 1000 to 8000 J g^{-1} [6, 7, 10]. Also, to our knowledge there are no data on enthalpy of formation and combustion of GO. Thirdly, GO has been reported to undergo dynamic aging

processes [37–41], whose effect on thermal decomposition reactivity and heat release are unknown. Finally, GO is a complex material, and work is needed to understand the role of partial reduction, salt impurities [6], and suspension pH prior to drying in the thermal decomposition process.

We address each of these issues by measuring quantitative thermochemical and kinetic parameters for GO thermal decomposition. Those kinetics are then used in a computational study of the sample sizes and environmental temperatures required to avoid self-heating and allow safe storage and processing that will be needed for successful nano-manufacturing of GO-based materials.

2. Experimental section

2.1. Materials

2.1.1. Graphite oxide (GO)—GO was prepared using a modified Hummers method and purified as described in our previous studies [5, 42]. Briefly, natural graphite powder was pre-treated with $K_2S_2O_8$ and P_2O_5 in concentrated H_2SO_4 and further oxidized with $KMnO_4$ in concentrated H_2SO_4 under continuous stirring. After a two-step washing with HCl and acetone, the product was dried under ambient atmosphere in dark. The GO product synthesized was stored in the form of bulk solid or GO cake. The GO powder was obtained by mechanical grinding of the GO cake to smaller pieces.

2.1.2. GO samples with additives—The desired mass of additive (KOH, KCl, ascorbate etc.) was weighed and transferred into a solution with fixed concentration by adding DI water. Then, the desired mass of solid GO was added into the premixed solution (with GO:additive mass ratio of 100:1). The mixture was agitated vigorously using a vortex mixer for approximately 30 seconds, after which, vials with GO plus salt solution were left uncapped in a 60°C oven overnight to dry. The resulting product is in the form of flaky powder.

2.2. Characterization

2.2.1. Morphology—The morphologies of all the materials used in this work were characterized with a LEO 1530 field-emission scanning electron microscope (SEM). The oxygen functional groups on the graphenic plane and edges were characterized using ATR accessory in Fourier Transform Infrared Spectroscopy (JASCO FT/IR-4100) and X-ray photoelectron spectroscopy (XPS) on Physical Electronics 5500 (PHI 5500) Multi-technique Surface Analyzer.

2.2.2. Thermal analysis—TA Instruments DSC-2910 Differential Scanning Calorimeter was applied to measure enthalpies of decomposition, and determine GO decomposition reaction onset temperatures. MT TGA/DSC-1 instrument was applied to test simultaneous mass loss and heat effects of GO. A heating rate of 10 K min^{-1} was used in most experiments, except in the kinetics experiments, where it was systematically varied to determine activation energy and frequency factor. The enthalpy of combustion of GO was determined by using Parr Instruments model 1421 semi-micro oxygen bomb calorimeter.

2.3. Decomposition kinetics and thermochemistry analysis

More detailed description of the analysis of the decomposition reaction kinetics and thermochemistry is offered in electronic supplementary information section of this work.

2.3.1. Decomposition reaction kinetics—Decomposition reaction rate constant activation energy and frequency factor were defined from variable heating rate DSC data applying Kissinger equation [43]

$$\ln\left(\frac{\phi}{{T_m}^2}\right) = \ln\left(\frac{AR}{E_a}\right) - \frac{E_a}{RT_m}, \quad (1)$$

where ϕ is heating rate, T_m is the temperature at which the heat flow reaches a maximum, A *is* frequency factor, E_a *is* activation energy. The empirical reaction order n was first estimated using Eq. (2) [43] and then verified by fitting isothermal DSC data with the kinetic model represented by Equations (1) and (2).

$$n = 1.26S^{0.5} \quad (2)$$

In Eq. (2), S is the curve shape index defined as the absolute value of the ratio of the slopes of tangents to the DSC curve at the two inflection points.

2.3.2. Self-heating analysis—Self-heating simulations were conducted applying the following energy balance equation

$$mC_p\frac{dT}{dt} = -m\Delta H\frac{dx}{dt} - hS(T - T_0), \quad (3)$$

where m is the mass of GO, C_p is the specific heat capacity, x is the mass fraction reacted, ΔH is the enthalpy of decomposition, h is the heat transfer coefficient to the local environment, T_0 is surrounding environment temperature (which was also taken to be the initial temperature of GO) and S is bulk GO external surface area, which is exposed to gas atmosphere. Adiabatic and non-adiabatic condition self-heating curves were computed applying numerical methods to Eq. (3), which details are found in electronic supplemental information.

2.3.3. Enthalpy of decomposition analysis—GO thermal reduction is essentially an organic disproportionation or decomposition reaction expressed as

$$\mathrm{GO} \rightarrow \mathrm{rGO} + \mathrm{CO_2} + \mathrm{CO} + \mathrm{H_2O}, \quad (4)$$

where rGO is solid reduced graphite oxide product. The enthalpy of decomposition for the reaction above can be estimated if the GO and rGO enthalpies of formation are known. In this work, we used the group contribution method, proposed by J. Marrero and R. Gani [44]

to obtain the GO enthalpy of formation for a variety of hypothetical GO organic structures. By introducing varying amounts of epoxides or hydroxyls to a polyaromatic (graphene) cluster with periodic boundaries, the quantitative contributions of these two types of groups to the GO enthalpy of formation is estimated. More details about these calculations can be found in electronic supplemental information section.

3. Results and discussion

3.1. GO thermal exfoliation in nitrogen and air atmospheres

Figure 1 illustrates the basic thermochemical behavior of GO upon slow heating at 10 K min^{-1}. In DSC under N_2 GO shows a small endotherm associated with water evaporation followed by a single exotherm corresponding to thermal decomposition with an onset temperature near 150°C and a total heat release of 1600 J g^{-1}. When heated in air, a second exotherm onset temperature also appears at ~ 550°C, which is a typical onset temperature for the oxidation of disordered or defective carbons prepared at low temperature [45, 46]. Integration of the higher-temperature peak gives a reaction enthalpy of 3920 J g^{-1}-initial-GO. This result is similar in magnitude to the standard heat of reaction for carbon (rGO) oxidation to CO: $C + 1/2O_2 \rightarrow CO$, which is 9200 J g^{-1}-C, and when renormalized to initial GO mass gives a value similar to the experimental result of 3900 J g^{-1} initial-GO-solid. The renormalization is performed by using GO C:O atomic ratio 2:1, and assuming the decomposition products as rGO, CO and CO_2 with CO:CO_2 ratio of 1:2 in gas products (CO:CO2 ratio based on study in Jung et al., 2009[47]).

We have also measured the total enthalpy of combustion of GO using an oxygen bomb calorimeter. Our duplicate experiments yielded a GO heat of combustion of 14,100 J g^{-1} initial-GO-solid, which is within a range of enthalpy of combustion for low calorie content solid fuels such as lignites, brown coals and biomasses. Based on our experimental measurements, theoretical predictions and literature review, it appears that the true decomposition enthalpy for GO is clearly in the range of 1000–2000 J g^{-1}, and the isolated reports of much higher values (~8000 J g^{-1}) may reflect studies carried out in air, which effectively report the sum of the decomposition enthalpy and further oxidation of either the char (rGO) or the gaseous decomposition products.

The smooth DSC heat decomposition curves in Figures 1A and 1B change to a truncated, asymmetric curve when larger sample size is used (see top curve on Figure 1B). This behavior is known to represent the explosive mode thermal decomposition, which occurs when GO decomposition reaction rate exceeds mass and heat transfer rates leading to local self-heating and thermal runaway reaction [5, 6, 10]. Both the sample mass and sample form (powder vs. consolidated “cake”) affect this transition (Figure 1B). While we are interested in the explosive events, and in ways to avoid them during processing and storage, the remainder of this study is carried out with relatively small size samples to achieve the non-explosive mode decomposition, which is required to obtain the smooth non-truncated heat curves needed to accurately measure and report quantitative kinetic and thermochemical parameters.

3.2. Role of salt impurities and reducing agents in GO decomposition reaction

Figure 2 explores the role of various salt impurities and chemical additives on GO thermal behavior. Potassium is a common impurity as a residue of the potassium permanganate used in graphite oxidation, and has been reported to promote ignition of GO upon heating [6]. Our previous study [5] reported that KOH addition reduced the onset temperature for GO thermal decomposition, and in some cases the initial portion of the exotherm extended down into the range of common drying operations (100–120°C). We have undertaken the study to understand the effect and the mechanism of KOH treatment, because such a low onset temperature raises special safety concerns. The new data in Figure 2A,B clearly show that the catalytic effect of KOH on GO decomposition is due to OH and not to K^+. Hydroxyl ion has been previously reported to be a catalyst for GO reduction in aqueous suspension [40], but this is the first report of its effect as a catalyst for GO thermal decomposition in dried samples. While K^+ does not effect GO thermal decomposition, it does catalyze the subsequent carbon (rGO) combustion reaction occurring at much higher temperatures (Figure 2C). Potassium addition reduces the onset temperature for $C+O_2 \rightarrow CO/CO_2$ by up to 200°C in Figure 2C, which is consistent with potassium's known role as an active char combustion catalyst [48–50]. These results indicate that when GO is heated in air, the presence of residual K^+ will not promote the original decomposition, but can increase the probability of subsequent ignition and rGO combustion with corresponding fire hazard [6] (Figure 2E).

The FTIR spectras in Figure 2D show that K^+ does not affect carbon-oxygen bonding in GO, but OH^- addition does, which may provide insight into its catalytic effects on decomposition. Specific peak interpretations for GO can be difficult due to overlapping features [40], but we can point out several specific alterations to the spectra upon OH^- addition. There is a decrease in intensity of the 1750 cm^{-1} shoulder peak (labeled "4") relative to the adjacent 1620 cm^{-1} peak, which is commonly associated with pristine graphenic domain C=C vibrations. This same change as been seen by Taniguchi et al [51], and the reduction in the 1750 cm^{-1} peak was suggested to be related to carboxyl groups that become reversibly quenched by K^+ binding in basic solution. Dimiev et al. [40] see a similar change in this peak ratio (1750/1620 cm^{-1}) with addition of base and assign it to differences in water content between the two samples. Base addition to GO increases or creates a peak at ~1350 cm^{-1} (labeled "3"), which could be C-OH [52], or carboxylic acid, O=C-OH [53]. In the C-O region from 900–1200 cm^{-1}, there is a decrease in the 970 cm^{-1} (labeled "1") shoulder peak (possibly epoxide) relative to the main 1042 cm^{-1} (labeled "2") peak representing various C-O structures [54]. These changes may represent epoxide ring-opening during chemical reduction, which is discussed in more detail later. At the same time we observed broadening of hydroxyl peak around 1040 cm^{-1}, indicating more complicated alcoholic structures form. These two changes imply the conversion from epoxides to hydroxyls during chemical reduction of GO.

Motivated by the observed effect of OH^-, we performed additional experiments to study pH effects more broadly. Figure 3A and B show that the pH of the original GO suspension has a strong effect on thermal decomposition kinetics. Increasing pH from 2 to 12 decreases the DSC peak onset temperature by over 50°C, which is a highly significant increase in GO

reactivity. Back-titration from pH=12 to pH=2 before drying reverses this effect – the low reactivity of the pH=2 product is restored, but only a fraction of the total exothermic heat (area under the curve) remains. This behavior suggests that OH^- catalyzes GO reduction in suspension, which has already been reported [55], but it further suggests that the partially reduced states captured by drying solid GO from pH=12 suspensions have an elevated thermal reactivity.

The molecular mechanism underlying the OH^- effect is not fully understood, but FTIR and XPS provide relevant information. Figure 3B shows reversible changes in the C1s XPS spectra upon pH change from 2 to 12 and back-titration to 2. Similar behavior has been reported by Tanigushi et al. [51] and interpreted as base-catalyzed epoxy ring opening reactions that are reversible on addition of acid. Reversible behavior is also seen in the FTIR spectra of Figure 3B – the spectral changes that occur on base addition, discussed already prior (and seen in Figure 2D), disappear upon back titration, and the pH=2 spectrum is essentially identical before and after the titration cycle. Taniguchi et al. present a theory for the reversible behavior based on pH-dependent epoxy ring opening/closing reactions [51]. Dimiev et al. also discuss base catalyzed epoxy ring opening reactions to form vicinal diols [40], which react further and irreversibly involving C-C bond cleavage and formation of vinylogous carboxylic acids. Further reaction in basic solution leads to CO_2 release, GO deoxygenation, and eventual degradation of GO into humic-like substances [40]. The present paper does not shed new insight into this molecular mechanism, but does show for the first time that these chemical transformations lead to increased thermal reactivity in GO when the intermediate, partially reduced states are captured by drying. This is consistent with the proposed mechanisms of base-catalyzed GO transformation, which involve defect creation during C-C bond breakage [40]. The elevated reactivity of partially reduced GO has important implications for the maximum allowed temperatures for safe processing of dry GO. A semi-global reaction scheme that is consistent with our data and the recent literature is shown in Figure 3D.

A series of experiments were carried out to test if only OH^- affects the thermal reactivity of dried GO, or if other chemical reducing agents have similar effects. Figure 3C shows a series of DSC traces on GO samples before and after incubation with a variety of chemical reducing agents (glutathione, ascorbic acid, citric acid, and Trolox). In each case, partial chemical reduction lowers the enthalpy of thermal decomposition, but raises the reactivity, seen as a lowering of the thermal decomposition onset temperature. The effect of base seen in Figure 3C appears to be a general effect of partial chemical reduction. In addition, $NaBH_4$ and hydrazine have also been tested, which exhibit similar effect (see Figure S1 in electronic supplemental information section). The elevated reactivity is seen when the chemical reducing agent is left in the dried GO, but also when it is removed by washing, though less significantly. This suggests that the source of the elevated rGO reactivity lies in the transformed chemical structure of the partially rGO, and not the presence of the chemical agent during heating.

3.3. Effect of GO aging

There have been several publications, which report that GO molecular structure evolves over the time during storage in the dry state or in suspension [37–41]. One study reports that GO aging involves loss of reactive epoxide groups [38]. However, it seems that epoxide groups are likely source of the high formation energy for GO structure, and therefore high decomposition energy (see our group contribution calculations results in Figure 4A). We thus initially suspected that aging would reduce the heat and/or reactivity associated with thermal decomposition. The results in Figure 4B show that in approximately three-month period this is not the case. Storage of GO in ambient conditions for up to 82 days has no significant effect on the decomposition enthalpy, and the reactivity shows a slight increase (measured as slight decrease in exotherm onset temperature). Therefore, exothermic decomposition and explosion hazards are not just features of freshly prepared GO, but also of aged GO stored up to at least several months.

3.4. Results of the decomposition kinetics analysis

Calculation methods are needed to define safe storage and processing conditions for a variety of sample sizes, shapes, and external environments. Such calculations require quantitative decomposition kinetics data, which we derive here from DSC data taken with systematic variation of heating rate. Results in Figure 5A show a regular shift in DSC trace with increasing heating rate. The kinetic analysis applied here is based on peak maximum temperature [43] recorded at each heating rate to give activation energy and frequency factor as defined in Eq. (1). The activation energy obtained in this work (142 kJ/mol) is similar to those reported previously using similar or different methods [47, 56]. By analyzing dynamic mode DSC data the apparent reaction order n was estimated to be 0.8. The latter value was then corrected to be 0.7, applying actual isothermal mode DSC data and the kinetic parameters determined earlier (see results in Figure 5C).

3.5. Discussion of results

Thermal reduction of GO is clearly a complex process, and results in Figures 1–5 provide some insight into molecular mechanism and have direct implications for safety in storage and processing. Thermal “reduction” is in reality thermal decomposition or pyrolysis process [57–59] and GO is unusual in that pyrolysis of oxygen-rich organic materials like coals and biomass is typically endothermic [60–64]. The annealing of oxidized carbon surfaces leading to deoxygenation (or devolatilization) is also usually endothermic [65], but there are exceptions for some oxidized carbon materials, for example ozonized fullerene and $KMnO_4$ oxidized carbon nanotubes [11, 66]. When compared with other common types of oxygen-containing carbon materials, the most significant structural differences of GO is the presence of large amount of epoxide [67], which are reactive groups with bond strain [38], and are not typically the primary functional group on carbon surfaces that are the result of reaction with ambient O_2. Our group contribution calculations (Figure 4A) suggest that epoxides are the source of the high formation energy of GO and thus its exothermic decomposition. A common feature of oxidized carbons that decompose exothermically appears to be the use of certain oxygen ring-creating oxidants like ozone, which forms highly reactive ozonides, or permanganate, which is a well-known catalyst for epoxide

formation in synthetic organic chemistry [68, 69]. Ozonized fullerene and $KMnO_4$ oxidized carbon nanotubes both show exothermic decomposition under heating [11, 66], which supports our calculation-based argument about the epoxide role in exothermic decomposition of GO.

This work further suggests that epoxides are involved in the complex response of GO to suspension pH. Base treatment renders GO more reactivity to thermal decomposition, and back titration to low pH partially reverses the effect. Reversible pH effects have been seen by Taniguchi are attributed to epoxide ring opening/closing [51], while the present paper shows for the first time that these reversible transformations also affect thermal decomposition reactivity. Drying GO from basic solutions can produce a more reactive solid product that begins to decompose at lower temperatures – in some cases down into the range of common drying operations, which can become a special safety concern. The reactive species may be vicinal diols resulting from epoxy ring opening, and these can further cleave to produce ketones or aldehydes [70]. Ketones and aldehydes are capable of further conversion to carboxyls under alkaline or thermal treatment [40, 71]. Diols can also be converted back to cyclic ethers including epoxides in acidic environments, leading to the partial reversibility shown in Figure 3D. The high thermal reactivity of the diol relative to epoxy is consistent with molecular dynamics and DFT simulations of GO thermal decomposition [41, 71] that show lower activation barriers for the initial step of OH decomposition compared to epoxy.

The observation of elevated thermal reactivity in partially reduced GO may be more general. It occurs not only following OH^- treatment but also for a variety of chemical reducing agents and reduction pathways (Figure 3C). Ahn et al. have also observed high reactivity in partially reduced GO samples [72].

As mentioned by previous theoretical studies [41, 71, 73], the energy of GO is lowered by clustering of the oxidized sites into domains, which co-exist with pristine sp^2 domains. Partial reduction here may break up the oxidized domains leading to more isolated oxygen-containing functional groups with high reactivity.

Of course, extensive or complete reduction eliminates the exotherm completely, as seen in results offered on Figure 1S (GO treatment with high concentration hydrazine). The phenomenon of elevated reactivity in GO samples after partial chemical reduction deserves further study.

Finally, the new kinetic parameters allow estimations of expected self-heating behavior relevant to industrial safety (Figure 6). An unsteady heat balance on a uniform GO mass gives the differential equation seen in Figure 6A, which can be solved numerically to give the predictions offered in Figure 6B,C. The simplest case is adiabatic self-heating, in which all of the reaction heat is retained in the GO body and the system always reaches the theoretical adiabatic temperature: $\Delta H = \Delta H/C_p$, which here is > 2,000°C for C_p around 0.5 J $g^{-1}K^{-1}$. The temperature behavior (see Figure 6B) shows first an incubation period of variable time length, followed by the temperature upturn, which leads to a thermal runaway. At room temperature the incubation times are very long, but at temperatures above ~150°C runaway can happen in minutes.

Adiabatic self-heating analysis is a crude estimate that only gives satisfactory result for fast processes that occur with short time for heat loss.

The results of non-adiabatic analysis are more practical. The method applies specific values of heat transfer coefficient (h) and the GO external surface area (S). In some cases this analysis gives a steady state temperature, while in other cases it gives an incubation period followed by an upturn and thermal runaway. Figure 6C plots the critical temperature T_c above, which the runaway occurs (and below which a steady-state temperature is achieved and no runaway) as a function of the initial bulk GO mass *m*. Some typical values for large and small GO forms (sample dimension in centimetres) and typical heat transfer coefficients (assuming GO to be a sphere) affecting critical temperature are shown in Figure 6C. As seen from this figure larger in size GO pieces have lower critical temperatures.

4. Conclusions

The energetic nature of GO was first identified long ago, but new research is needed to understand the phenomenon at a level that will allow safe management of GO during the large-scale nano-manufacturing of graphene-based materials. This article presents an experimental characterization of the thermochemistry of GO, and reports quantitative values for the enthalpy of combustion, the enthalpy of thermal decomposition, the rates of thermal decomposition, and their dependence on temperature, GO composition, and processing history. GO decomposition is shown to be accelerated by partial chemical reduction, or by exposure to high-pH conditions in suspension prior to drying. Transformations of epoxide groups are suggested as the cause of the exothermic decomposition and the reversible effects of acid/base treatment. Residual potassium does not catalyze GO decomposition, but rather catalyzes the subsequent heterogeneous combustion of the rGO carbon product. This body of data suggests that large samples of GO in some storage and handling scenarios will be capable of self-heating and spontaneous decomposition leading to high-volume gas release and explosive events. The quantitative kinetic parameters reported here can be used to identify safe conditions for storage and handling, and to identify compositions and processing protocols that will help ensure the successful transition of GO-based graphene materials from laboratory subjects to commodity products.

Supplementary Material

Refer to Web version on PubMed Central for supplementary material.

Acknowledgments

This work was supported by the Superfund Research Program of the National Institute of Environmental Health Sciences (Grant P42 ES013660).

References

1. Brodie BC. On the atomic weight of graphite. Philosophical Transactions of the Royal Society of London. 1859:249–259.
2. Scholz W, Boehm HP. Die Thermische Zersetzung Von Graphitoxyd. Naturwissenschaften. 1964; 51(7):160.

3. Boehm HP, Scholz W. Der Verpuffungspunkt Des Graphitoxids. Zeitschrift Fur Anorganische Und Allgemeine Chemie. 1965; 335(1–2):74.
4. Boehm HP, Clauss A, Fischer GO, Hofmann U. Das Adsorptionsverhalten Sehr Dunner Kohlenstoff-Folien. Zeitschrift Fur Anorganische Und Allgemeine Chemie. 1962; 316(3–4):119–127.
5. Qiu Y, Guo F, Hurt R, Külaots I. Explosive thermal reduction of graphene oxide-based materials: Mechanism and safety implications. Carbon. 2014; 72(0):215–223. [PubMed: 25018560]
6. Kim F, Luo JY, Cruz-Silva R, Cote LJ, Sohn K, Huang JX. Self-Propagating Domino-like Reactions in Oxidized Graphite. Advanced Functional Materials. 2010; 20(17):2867–2873.
7. Krishnan D, Kim F, Luo JY, Cruz-Silva R, Cote LJ, Jang HD, et al. Energetic graphene oxide: Challenges and opportunities. Nano Today. 2012; 7(2):137–152.
8. Botas C, Alvarez P, Blanco C, Santamaria R, Granda M, Gutierrez MD, et al. Critical temperatures in the synthesis of graphene-like materials by thermal exfoliation-reduction of graphite oxide. Carbon. 2013; 52:476–485.
9. You SJ, Luzan SM, Szabo T, Talyzin AV. Effect of synthesis method on solvation and exfoliation of graphite oxide. Carbon. 2013; 52:171–180.
10. McAllister MJ, Li JL, Adamson DH, Schniepp HC, Abdala AA, Liu J, et al. Single sheet functionalized graphene by oxidation and thermal expansion of graphite. Chemistry of Materials. 2007; 19(18):4396–4404.
11. Cataldo F, Compagnini G, D'Urso L, Palleschi G, Valentini F, Angelini G, et al. Characterization of Graphene Nanoribbons from the Unzipping of MWCNTs. Fullerenes Nanotubes and Carbon Nanostructures. 2010; 18(3):261–272.
12. Jimenez PSV. Thermal-Decomposition of Graphite Oxidation-Products Dsc Studies of Internal-Combustion of Graphite Oxide. Materials Research Bulletin. 1987; 22(5):601–608.
13. Boehm, H.; Clauss, A.; Fischer, G.; Hofmann, U. Surface properties of extremely thin graphite lamellae. Proceedings of the fifth Conference on Carbon: Pergamon Press; p. 73-80.
14. Novoselov KS, Jiang D, Schedin F, Booth TJ, Khotkevich VV, Morozov SV, et al. Two-dimensional atomic crystals. Proceedings of the National Academy of Sciences of the United States of America. 2005; 102(30):10451–10453. [PubMed: 16027370]
15. Novoselov KS, Geim AK, Morozov SV, Jiang D, Zhang Y, Dubonos SV, et al. Electric field effect in atomically thin carbon films. Science. 2004; 306(5696):666–669. [PubMed: 15499015]
16. Geim AK, Novoselov KS. The rise of graphene. Nature Materials. 2007; 6(3):183–191. [PubMed: 17330084]
17. Chen CM, Yang QH, Yang YG, Lv W, Wen YF, Hou PX, et al. Self-Assembled Free-Standing Graphite Oxide Membrane. Advanced Materials. 2009; 21(29):3007-+.
18. Kim J, Cote LJ, Kim F, Yuan W, Shull KR, Huang JX. Graphene Oxide Sheets at Interfaces. Journal of the American Chemical Society. 2010; 132(23):8180–8186. [PubMed: 20527938]
19. Xu YX, Sheng KX, Li C, Shi GQ. Self-Assembled Graphene Hydrogel via a One-Step Hydrothermal Process. Acs Nano. 2010; 4(7):4324–4330. [PubMed: 20590149]
20. Huang H, Chen PW, Zhang XT, Lu Y, Zhan WC. Edge-to-Edge Assembled Graphene Oxide Aerogels with Outstanding Mechanical Performance and Superhigh Chemical Activity. Small. 2013; 9(8):1397–1404. [PubMed: 23512583]
21. Zhao GX, Li JX, Ren XM, Chen CL, Wang XK. Few-Layered Graphene Oxide Nanosheets As Superior Sorbents for Heavy Metal Ion Pollution Management. Environmental Science & Technology. 2011; 45(24):10454–10462. [PubMed: 22070750]
22. Stankovich S, Dikin DA, Dommett GHB, Kohlhaas KM, Zimney EJ, Stach EA, et al. Graphene-based composite materials. Nature. 2006; 442(7100):282–286. [PubMed: 16855586]
23. Singh VK, Shukla A, Patra MK, Saini L, Jani RK, Vadera SR, et al. Microwave absorbing properties of a thermally reduced graphene oxide/nitrile butadiene rubber composite. Carbon. 2012; 50(6):2202–2208.
24. Zhu XJ, Zhu YW, Murali S, Stollers MD, Ruoff RS. Nanostructured Reduced Graphene Oxide/Fe2O3 Composite As a High-Performance Anode Material for Lithium Ion Batteries. Acs Nano. 2011; 5(4):3333–3338. [PubMed: 21443243]

25. Zhang C, Lv W, Xie X, Tang D, Liu C, Yang Q-H. Towards low temperature thermal exfoliation of graphite oxide for graphene production. Carbon. 2013; 62:11–24.
26. Chen GH, Weng WG, Wu DJ, Wu CL. PMMA/graphite nanosheets composite and its conducting properties. Eur Polym J. 2003; 39(12):2329–2335.
27. Göktürk HS, Fiske TJ, Kalyon DM. Effects of particle shape and size distributions on the electrical and magnetic properties of nickel/polyethylene composites. J Appl Polym Sci. 1993; 50(11):1891–1901.
28. Fiori G, Bonaccorso F, Iannaccone G, Palacios T, Neumaier D, Seabaugh A, et al. Electronics based on two-dimensional materials. Nature Nanotechnology. 2014; 9(10):768–779.
29. Liu J. Charging graphene for energy. Nature Nanotechnology. 2014; 9(10):739–741.
30. Torrisi F, Coleman JN. Electrifying inks with 2D materials. Nature Nanotechnology. 2014; 9(10): 738–739.
31. Ahn JH, Hong BH. Graphene for displays that bend. Nature Nanotechnology. 2014; 9(10):737–738.
32. Bohm S. Graphene against corrosion. Nature Nanotechnology. 2014; 9(10):741–742.
33. Zhang XY, Huang Y, Wang Y, Ma YF, Liu ZF, Chen YS. Synthesis and characterization of a graphene-C-60 hybrid material. Carbon. 2009; 47(1):334–337.
34. Becerril HA, Mao J, Liu Z, Stoltenberg RM, Bao Z, Chen Y. Evaluation of solution-processed reduced graphene oxide films as transparent conductors. Acs Nano. 2008; 2(3):463–470. [PubMed: 19206571]
35. Senthilkumaar S, Varadarajan PR, Porkodi K, Subbhuraam CV. Adsorption of methylene blue onto jute fiber carbon: kinetics and equilibrium studies. Journal of colloid and interface science. 2005; 284(1):78–82. [PubMed: 15752787]
36. Watcharotone S, Dikin DA, Stankovich S, Piner R, Jung I, Dommett GHB, et al. Graphene-silica composite thin films as transparent conductors. Nano letters. 2007; 7(7):1888–1892. [PubMed: 17592880]
37. Chua CK, Pumera M. Light and atmosphere affect the Quasi-equilibrium states of graphite oxide and graphene oxide powders. Small. 2015; 11(11):1266–1272. [PubMed: 25332199]
38. Kim S, Zhou S, Hu YK, Acik M, Chabal YJ, Berger C, et al. Room-temperature metastability of multilayer graphene oxide films. Nature Materials. 2012; 11(6):544–549. [PubMed: 22561900]
39. Pendolino F, Parisini E, Lo Russo S. Time-Dependent Structure and Solubilization Kinetics of Graphene Oxide in Methanol and Water Dispersions. J Phys Chem C. 2014; 118(48):28162–28169.
40. Dimiev AM, Alemany LB, Tour JM. Graphene oxide. Origin of acidity, its instability in water, and a new dynamic structural model. Acs Nano. 2013; 7(1):576–588. [PubMed: 23215236]
41. Zhou S, Bongiorno A. Origin of the chemical and kinetic stability of graphene oxide. Sci Rep. 2013; 3:2484. [PubMed: 23963517]
42. Qiu Y, Wang Z, Owens ACE, Kulaots I, Chen Y, Kane AB, et al. Antioxidant chemistry of graphene-based materials and its role in oxidation protection technology. Nanoscale. 2014; 6(20): 11744–11755. [PubMed: 25157875]
43. Kissinger HE. Reaction Kinetics in Differential Thermal Analysis. Analytical Chemistry. 1957; 29(11):1702–1706.
44. Marrero J, Gani R. Group-contribution based estimation of pure component properties. Fluid Phase Equilibria. 2001; 183:183–208.
45. Henrich E, Burkle S, Meza-Renken ZI, Rumpel S. Combustion and gasification kinetics of pyrolysis chars from waste and biomass. Journal of Analytical and Applied Pyrolysis. 1999; 49(1–2):221–241.
46. Stanmore BR, Brilhac JF, Gilot P. The oxidation of soot: a review of experiments, mechanisms and models. Carbon. 2001; 39(15):2247–2268.
47. Jung I, Field DA, Clark NJ, Zhu YW, Yang DX, Piner RD, et al. Reduction Kinetics of Graphene Oxide Determined by Electrical Transport Measurements and Temperature Programmed Desorption. J Phys Chem C. 2009; 113(43):18480–18486.

48. Antal MJ, Gronli M. The art, science, and technology of charcoal production. Industrial & Engineering Chemistry Research. 2003; 42(8):1619–1640.
49. Jones JM, Darvell LI, Bridgeman TG, Pourkashanian M, Williams A. An investigation of the thermal and catalytic behaviour of potassium in biomass combustion. Proceedings of the Combustion Institute. 2007; 31:1955–1963.
50. Jensen A, Dam-Johansen K, Wojtowicz MA, Serio MA. TG-FTIR study of the influence of potassium chloride on wheat straw pyrolysis. Energy & Fuels. 1998; 12(5):929–938.
51. Taniguchi T, Kurihara S, Tateishi H, Hatakeyama K, Koinuma M, Yokoi H, et al. pH-driven, Reversible Epoxy Ring Opening/Closing in Graphene Oxide. Carbon. 2015; 84:560–566.
52. Yan XB, Chen JT, Yang J, Xue QJ, Miele P. Fabrication of Free-Standing, Electrochemically Active, and Biocompatible Graphene Oxide-Polyaniline and Graphene-Polyaniline Hybrid Papers. Acs Applied Materials & Interfaces. 2010; 2(9):2521–2529. [PubMed: 20735069]
53. Acik M, Lee G, Mattevi C, Pirkle A, Wallace RM, Chhowalla M, et al. The Role of Oxygen during Thermal Reduction of Graphene Oxide Studied by Infrared Absorption Spectroscopy. The Journal of Physical Chemistry C. 2011; 115(40):19761–19781.
54. Xu JJ, Wang K, Zu SZ, Han BH, Wei ZX. Hierarchical Nanocomposites of Polyaniline Nanowire Arrays on Graphene Oxide Sheets with Synergistic Effect for Energy Storage. Acs Nano. 2010; 4(9):5019–5026. [PubMed: 20795728]
55. Fan XB, Peng WC, Li Y, Li XY, Wang SL, Zhang GL, et al. Deoxygenation of Exfoliated Graphite Oxide under Alkaline Conditions: A Green Route to Graphene Preparation. Advanced Materials. 2008; 20(23):4490–4493.
56. Kuibo Y, Haitao L, Yidong X, Hengchang B, Jun S, Zhiguo L, et al. Thermodynamic and kinetic analysis of low-temperature thermal reduction of graphene oxide. Nano-Micro Letters. 2011; 3(1): 51–55.
57. Lin ZY, Waller G, Liu Y, Liu ML, Wong CP. Facile Synthesis of Nitrogen-Doped Graphene via Pyrolysis of Graphene Oxide and Urea, and its Electrocatalytic Activity toward the Oxygen-Reduction Reaction. Advanced Energy Materials. 2012; 2(7):884–888.
58. Stankovich S, Dikin DA, Piner RD, Kohlhaas KA, Kleinhammes A, Jia Y, et al. Synthesis of graphene-based nanosheets via chemical reduction of exfoliated graphite oxide. Carbon. 2007; 45(7):1558–1565.
59. Compton OC, Nguyen ST. Graphene Oxide, Highly Reduced Graphene Oxide, and Graphene: Versatile Building Blocks for Carbon-Based Materials. Small. 2010; 6(6):711–723. [PubMed: 20225186]
60. Mahajan OP, Tomita A, Walker PL. Differential Scanning Calorimetry Studies on Coal.1. Pyrolysis in an Inert Atmosphere. Fuel. 1976; 55(1):63–69.
61. Mohan D, Pittman CU, Steele PH. Pyrolysis of wood/biomass for bio-oil: A critical review. Energy & Fuels. 2006; 20(3):848–889.
62. Antal MJ, Varhegyi G. Cellulose Pyrolysis Kinetics - the Current State Knowledge. Industrial & Engineering Chemistry Research. 1995; 34(3):703–717.
63. Bradbury AGW, Sakai Y, Shafizadeh F. A kinetic model for pyrolysis of cellulose. Journal of Applied Polymer Science. 1979; 23(11):3271–3280.
64. Kok MV, Ozbas E, Karacan O, Hicyilmaz C. Effect of particle size on coal pyrolysis. Journal of Analytical and Applied Pyrolysis. 1998; 45(2):103–110.
65. Milosavljevic I, Oja V, Suuberg EM. Thermal effects in cellulose pyrolysis: Relationship to char formation processes. Industrial & Engineering Chemistry Research. 1996; 35(3):653–662.
66. Heymann D, Bachilo SM, Weisman RB, Cataldo F, Fokkens RH, Nibbering NMM, et al. C60O3, a fullerene ozonide: Synthesis end dissociation to C60O and O-2. Journal of the American Chemical Society. 2000; 122(46):11473–11479.
67. Lerf A, He HY, Forster M, Klinowski J. Structure of graphite oxide revisited. Journal of Physical Chemistry B. 1998; 102(23):4477–4482.
68. Hanson JR, Hitchcock PB, Liman MD, Nagaratnam S, Manickavasagar R. The Stereochemistry of Epoxidation of Some Steroidal Alkenes with Potassium Permanganate-Copper Sulfate. Journal of Chemical Research-S. 1995; (6):220–221.

69. Hanson JR, Terry N, Uyanik C. The stereochemistry of epoxidation of Delta(5)-steroids with sodium perborate and potassium permanganate. Journal of Chemical Research-S. 1998; (1):50–51.

70. Nicoli BH, Shinn LA. The action of periodic acid on alpha-amino alcohols. Journal of the American Chemical Society. 1939; 61:1615-.

71. Bagri A, Mattevi C, Acik M, Chabal YJ, Chhowalla M, Shenoy VB. Structural evolution during the reduction of chemically derived graphene oxide. Nature Chemistry. 2010; 2(7):581–587.

72. Ahn SI, Kim K, Kim JY, Kim ES, Han JY, Eom JW, et al. Reduction intermediates of graphene oxide for low temperature reduction electrode material. RSC Advances. 2014; 4(43):22476.

73. Larciprete R, Fabris S, Sun T, Lacovig P, Baraldi A, Lizzit S. Dual path mechanism in the thermal reduction of graphene oxide. J Am Chem Soc. 2011; 133(43):17315–17321. [PubMed: 21846143]

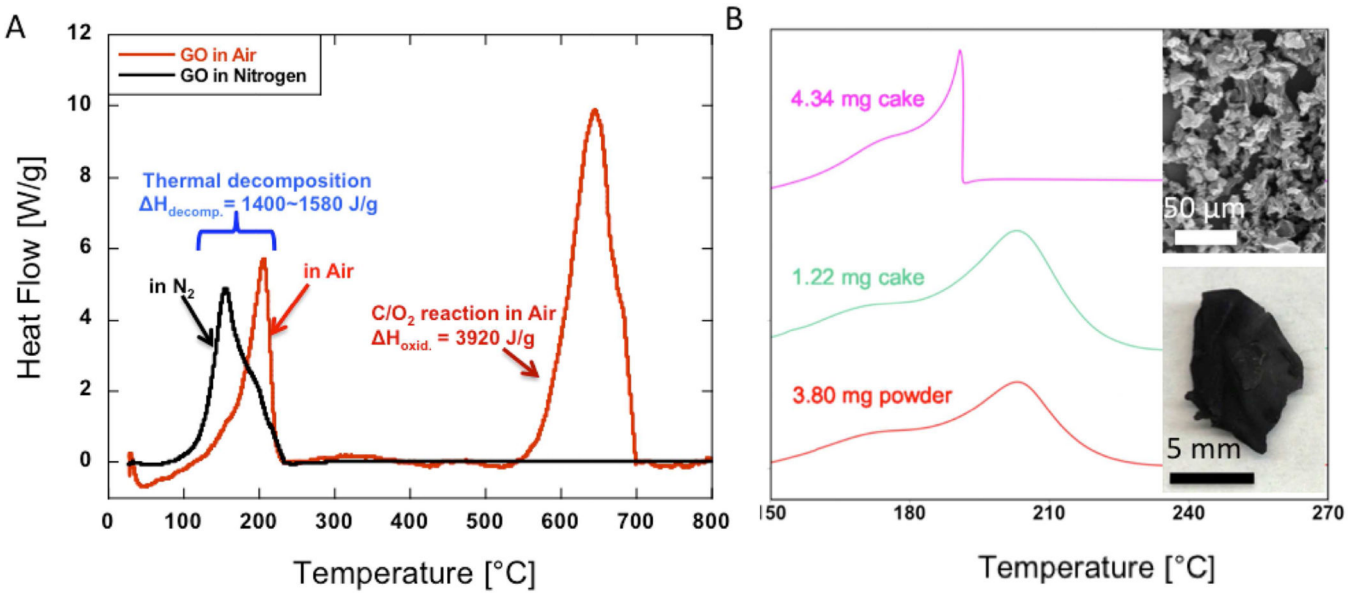

Fig. 1.

(A) DSC thermograms of GO thermal reduction in nitrogen compared with the same sample reduction and oxidation in air. (B) GO cake and GO powder thermograms heated in nitrogen atmosphere. GO powder is obtained by mechanical grinding of the GO cake to smaller pieces. The GO initial mass and solid form (powder versus single large piece) determine if the decomposition of GO occurs in explosive or non-explosive modes. The non-explosive thermal reduction produces a large rGO monolith similar to the starting form of the GO cake (lower inset image), while the explosive mode produces rGO in the form of micron-sized particles (upper inset image).

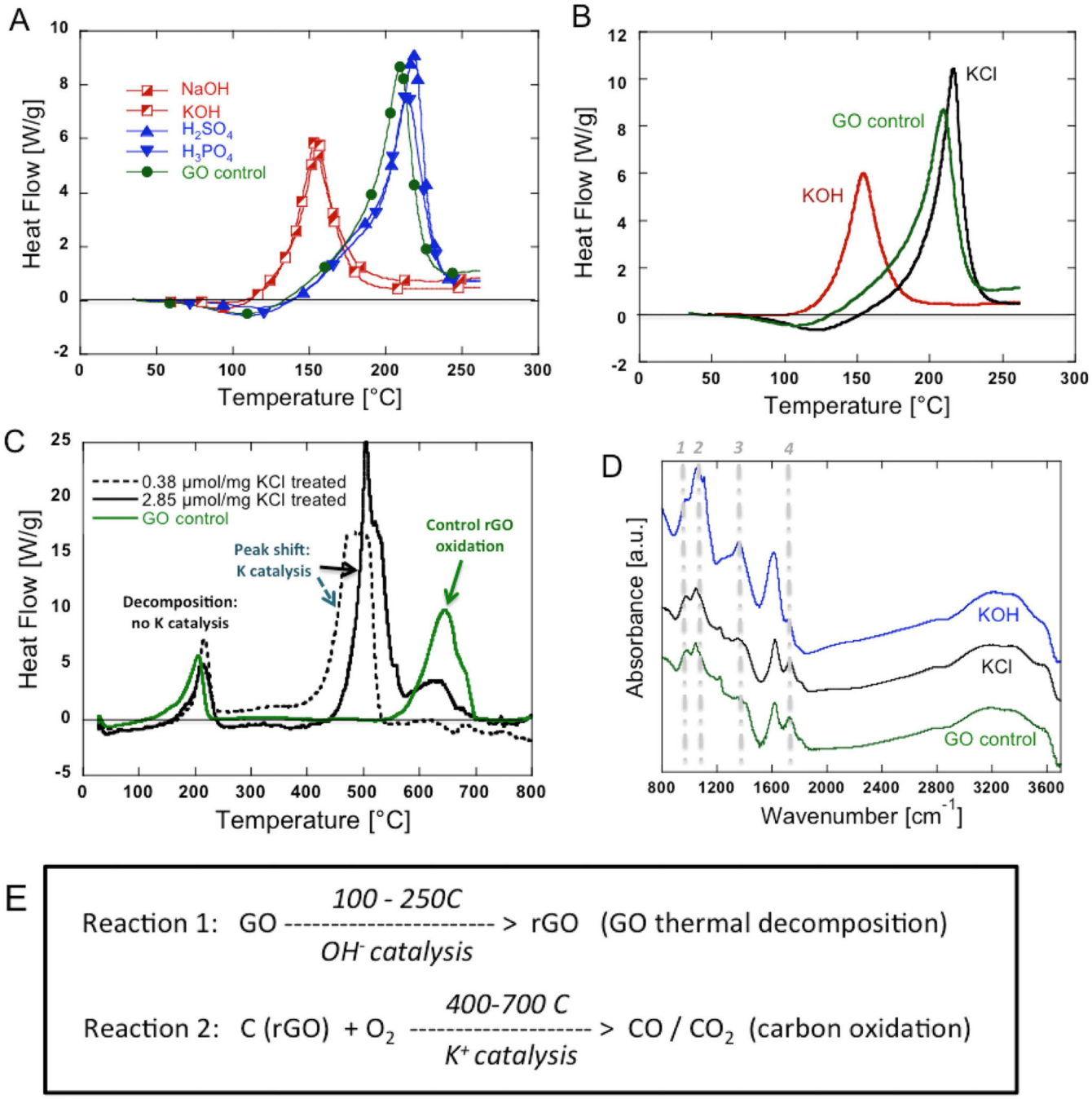

Fig. 2.

Role of salt impurities on GO decomposition and rGO combustion kinetics. Samples were prepared by adding salts, bases, or acids into GO suspensions (GO:additive = 100:1 by mass) and dried overnight at 60°C in air. (A, B) DSC thermograms show that K^+ does not catalyze GO thermal decomposition, but OHdoes. (C) DSC thermograms on GO with salt additives in non-hermetic DSC pan in air. K^+ does not affect GO decomposition, but strongly catalyzes rGO combustion at higher temperature. (D) FTIR spectra of GO and GO with salt additives. KCl addition has no effect on the spectrum, while KOH addition alters

several peaks associated with C-O or C=O bonding. (E) Global reactions in GO thermal behavior.

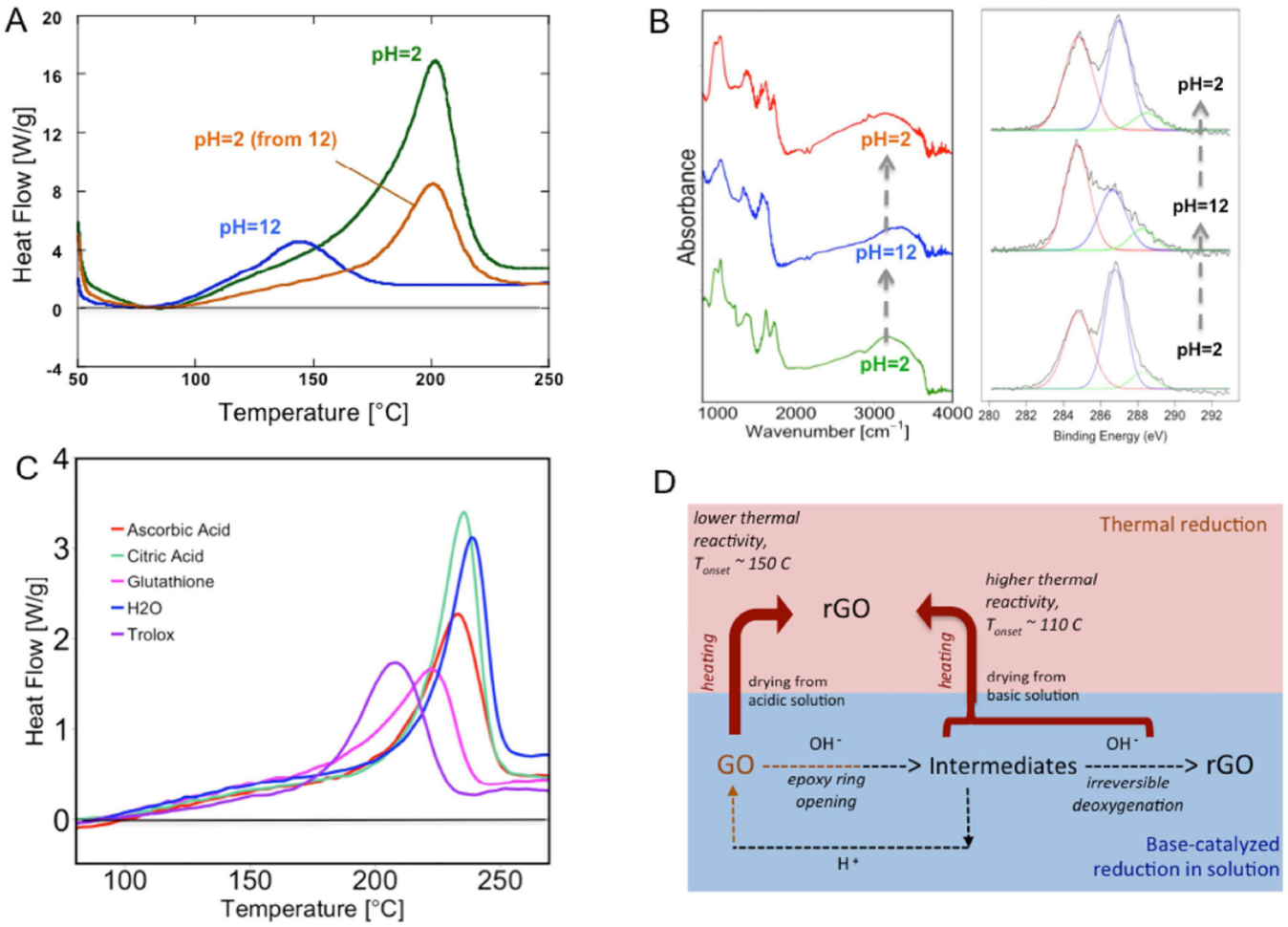

Fig. 3.

pH effects on the structural and thermal behavior of GO. The GO samples used for these characterizations are recovered and dried from suspension stored at different pH's. (A) DSC thermograms of acidic and basic GOs. Base treatment to pH = 12 reduces GO, however lowers significantly decomposition onset temperature down to ~100°C. Same GO back treatment to pH = 2 increases enthalpy of decomposition, hence the total heat is still less than original pH = 2 GO heat of decomposition. Onset temperature moves back to ~150°C after acid treatment of GO. (B) FTIR and XPS spectras of acid and based-treated GO samples. GO base treatment to pH = 12 reduces FTIR peaks at 1050 cm^{-1}, 970 cm^{-1}, 1754 cm^{-1} groups. GO recovered from pH = 2, back treated from pH = 12 exhibits similar but not identical functionalities as pH = 2. The de-convoluted peaks in XPS spectra are C-C/C=C (red), C-O (blue) and C=C (green), respectively. Similar to FTIR, GO back titrated from pH = 12 to pH=2 exhibits similar but not identical functionalities as initial pH = 2 sample. (C) DSC thermograms of common weak reducing agent treated GOs. The decomposition reaction onset temperature is lowered in all four cases. (D) A semi-global kinetic structure of the coupled thermal and base-catalyzed reduction of GO: pH of precursor suspension influences reactivity and safety of thermal reduction.

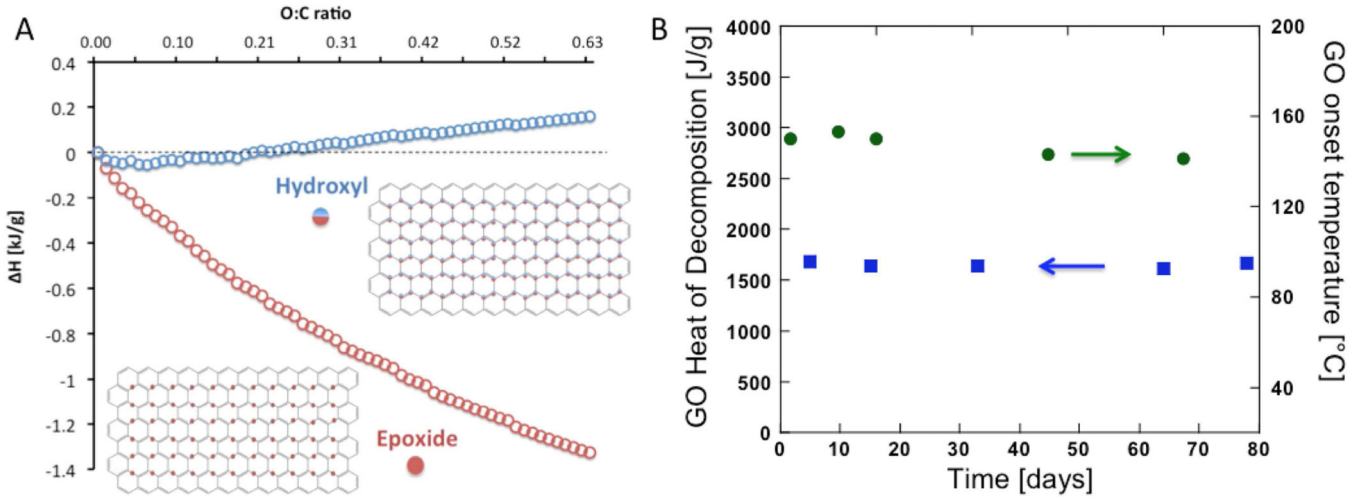

Fig. 4.

(A) Theoretical decomposition enthalpies of potential GO structures with varying O:C ratio, and the amount of either epoxides (structure shown in lower left inset) or hydroxyls (structure shown in upper right inset) estimated applying calculated enthalpies of formation of GO (from group contribution method). Increasing epoxide content makes GO decomposition significantly more exothermic, while increasing hydroxyl content makes GO decomposition slightly endothermic. (B) The effect of GO aging on thermal decomposition enthalpy and reactivity. In approximately three months time frame GO aging dose not significantly affect the decomposition enthalpy but does slightly lower the GO onset temperature.

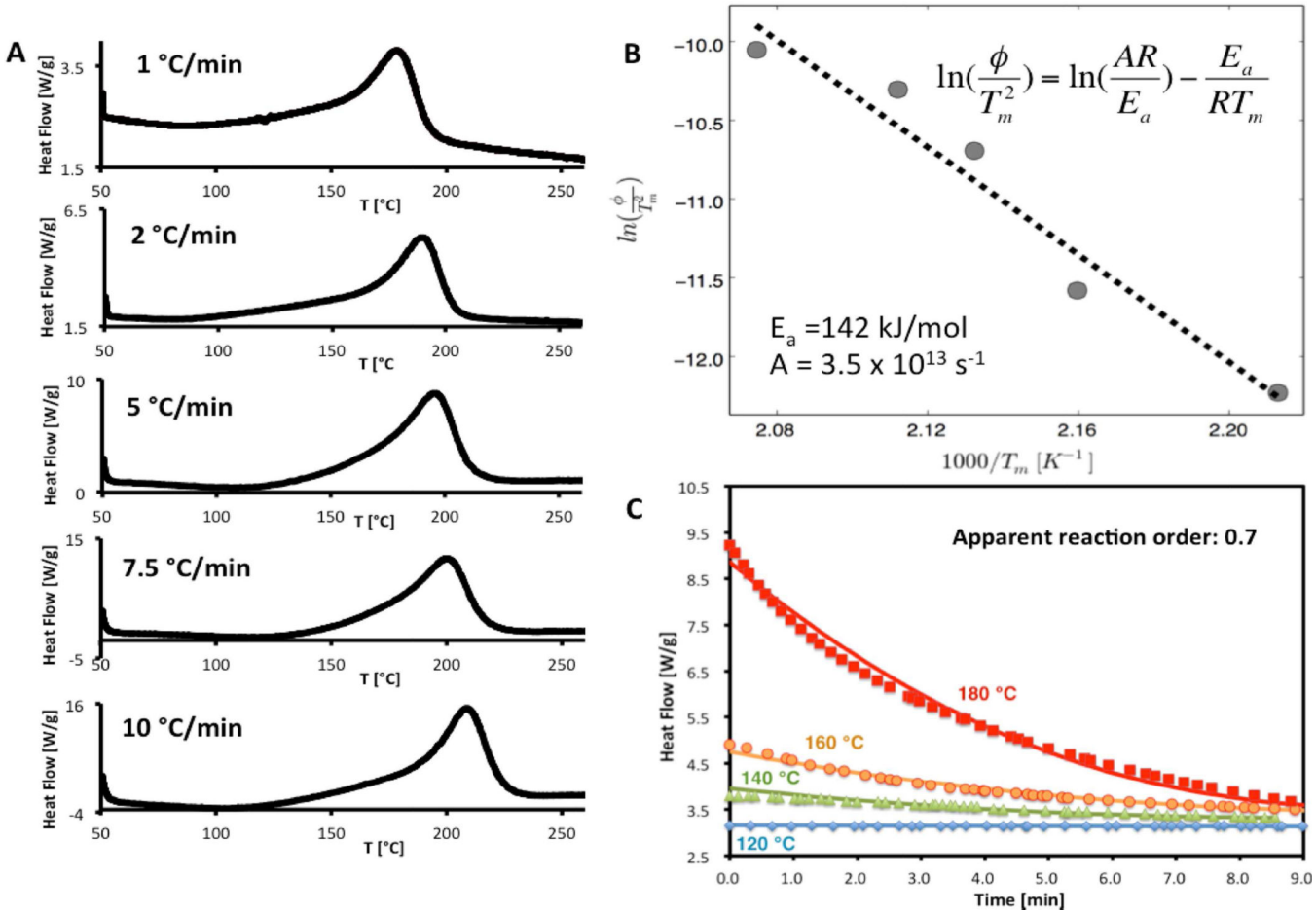

Fig. 5.

Quantitative determination of GO thermal decomposition kinetics. The GO used here is as-prepared GO stored at room temperature in atmosphere. The experiments were carried out with small sample sizes to avoid the explosive mode of decomposition. (A) Dynamic mode DSC thermograms with systematic variation in heating rate. (B) Extraction of quantitative kinetics parameters. (C) Validation of theoretical kinetic data obtained (activation energy, pre-exponential factor and rate order). Experimental isothermal DSC data (data points) compared with the theoretical curve (solid line). The determined kinetic model matches well with experimental data.

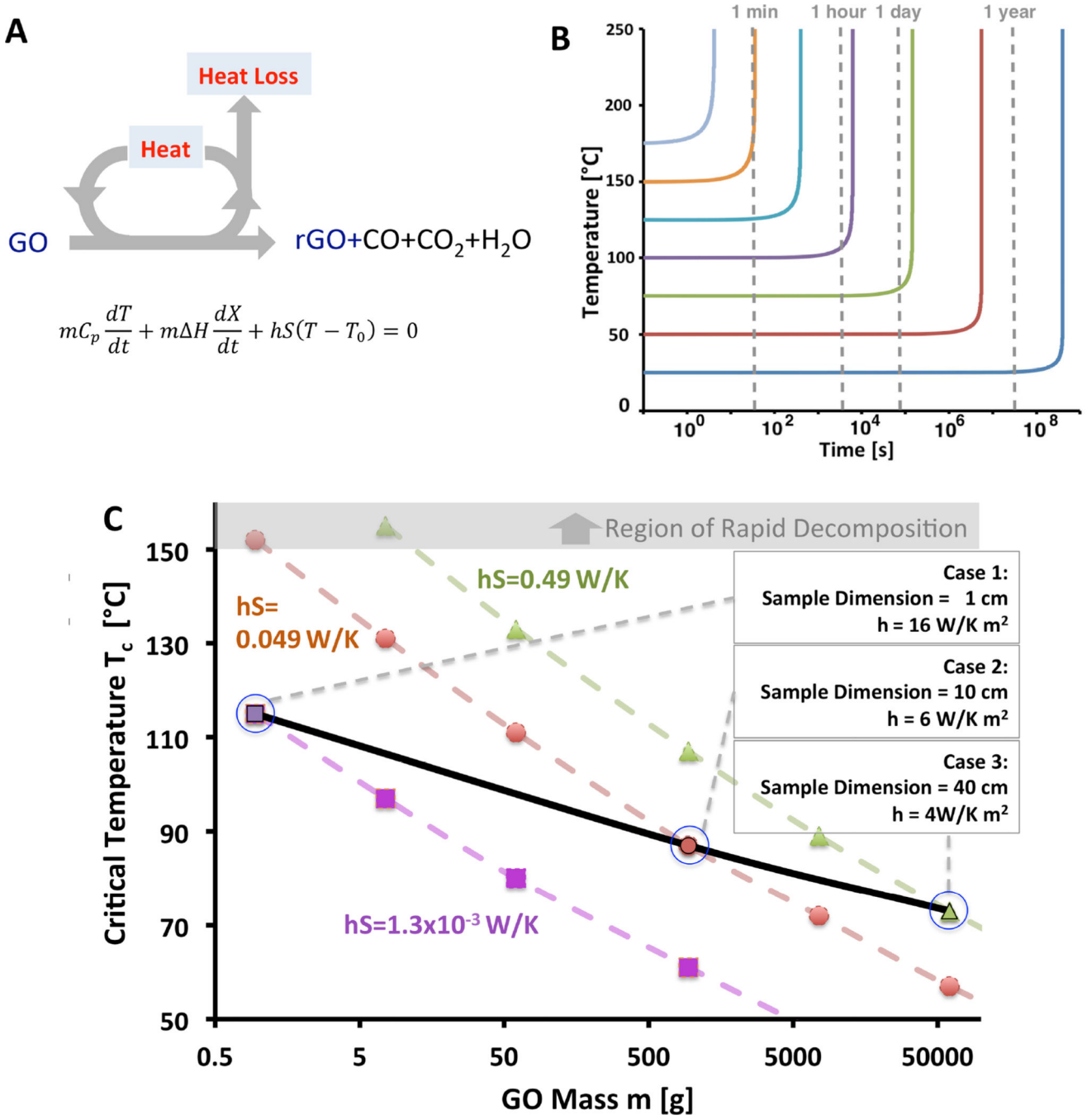

Fig. 6.

Information on self-heating behavior of large GO samples relevant to manufacturing safety. (A) Differential energy balance and decomposition mechanism (B) Temperature curves for numerical solutions for adiabatic self-heating case, (C) T_c vs m for non-adiabatic self-heating cases as a function of heat transfer coefficient and surface area product, hS; T_c is the critical initial temperature above which the runaway occurs and below which a steady-state temperature is achieved; m, the mass of GO; h, the heat transfer coefficient; S, the external surface area. GO with greater mass and smaller value of hS is more likely to reach the point

of no return to initiate the thermal runaway reaction. Three example cases are shown with different sample dimensions and associated typical heat transfer coefficients when heat convection from the GO surface to the environment is the rate limiting in heat transfer mechanism.